Atomistic Molecular Dynamics Simulation of Polydisperse Linear Polyethylene Melts

Vagelis A. Harmandaris, Vlasis G. Mavrantzas, and Doros N. Theodorou*

Department of Chemical Engineering, University of Patras, GR 26500 Patras, Greece, and Institute of Chemical Engineering and High Temperature Chemical Processes, GR 26500 Patras, Greece

Received May 1, 1998; Revised Manuscript Received August 13, 1998

ABSTRACT: Well-relaxed atomistic configurations of polydisperse, linear polyethylene (PE) melts, obtained with the end-bridging Monte Carlo algorithm, have been subjected to detailed molecular dynamics simulations in both the canonical (*NVE*) and microcanonical (*NVT*) ensembles. Three different systems have been investigated, characterized by mean molecular lengths C_{24}, C_{78}, and C_{156}, and by the same polydispersity index *I* of about 1.09. Results are presented for the static and (mainly) dynamic properties of these melts at $P = 1$ atm and $T = 450$ K. The diffusion coefficient *D*, determined for various chain lengths, *N*, is in very good agreement with experimentally measured values. The friction coefficient ζ_D is extracted from *D* by invoking the Rouse model; it is seen to increase from a relatively small value characteristic of short alkanes to a chain-length-independent plateau, reached in a region of $N = 60-80$. The friction coefficient ζ_τ is also obtained by analyzing the decay of the time autocorrelation function for the normal modes $\mathbf{X}_p$ at various chain lengths; the values thus extracted are consistent with those obtained from *D* for *N* above 40. Although the decay of the autocorrelation function of the end-to-end vector is very well described by the Rouse model, individual Rouse modes show some deviation from theoretical predictions. Even for chains sufficiently long to be in the asymptotic ζ regime, only the first two normal modes fully conform to Rouse theory in terms of their squared amplitudes and correlation times. Zero-shear viscosities computed from ζ_D values by means of the Rouse model are in excellent agreement with available experimental data for $N = 90$.

1. Introduction

The design of efficient and reliable molecular modeling techniques for predicting the physical properties of polymers from chain chemical constitution is a challenging but worthwile objective. In particular, modeling dynamic properties in the molten state is of great significance in all polymer-processing industries, since these properties govern the processability of the melts. This explains the recent increased interest in dynamic simulations of chain liquids, particularly of systems composed of longer chain molecules or molecules with a more complex than linear architecture.

The molecular dynamics (MD) technique, despite its inherent limitations in vigorously sampling the configuration space of highly connected, dense systems, has continued to be the dominant method in the area and has enjoyed extensive use in the last few years. This is not only because of the simplicity of the method, but also because of its unique capability to provide direct information on the temporal evolution of the system, a feature that the other large class of molecular simulations, Monte Carlo (MC), lacks.[1,2] Recently, MD has been used to study the dynamics of a number of systems, ranging from simple fluids and alkanes to polymer chains and networks.[3]

The most serious problem faced by MD of long chain systems is that the time span tracked in the course of the simulation is very short in comparison to the spectrum of times characterizing molecular motions in these systems. The longest relaxation time of even relatively short chain melts (e.g., C_{100} to C_{200}), increases strongly with chain length and can well exceed the time intervals that can be simulated with today's supercomputers. To overcome this serious limitation, either simulations are limited to shorter chains, or coarse-grained models are invoked to scale-up the time.[3] A widely used coarse-grained model is the bead-spring chain model.[4] Simulations with this model have been reported for systems with chains up to 200 beads long.[5]

The first atomistic MD simulations of chain molecules considered small alkanes,[6] such as C_4 and C_8, and mainly focused on static properties. With the new generations of powerful computers, both the model systems considered and the constituent molecules increased substantially in size and length. The limit of 10 ns, which was very difficult to track a few years ago, even for systems consisting of a small number of short chain molecules, is now easily accesible, and simulations on the order of 90 ns have been reported for very large systems as, for example, a system containing 640 chains with $N = 100$ carbon atoms per chain.[7,8] In parallel, the technique of nonequilibrium molecular dynamics (NEMD) has gained ground, mainly because of its advantage in calculating viscosity by imposing a shear flow (usually the Couette flow) on the system.[9−12] However, as with equilibrium MD, the long relaxation time problem is also encountered with NEMD when the simulation is pushed to rather long chains. Huge shear rates are usually applied, and the zero shear-rate viscosity is only calculable by extrapolation to the low shear-rate regime.[10]

Recently, Mondello and Grest[13] have calculated the zero-shear rate viscosity η_0 through both the Green−Kubo relation and the Rouse model for small alkanes (C_n, $n < 16$). In a systematic study over the last few years, Yoon and collaborators[14−17] have also reported results from long MD simulations on three different

* Author to whom correspondence should be addressed at the University of Patras (telephone, +3061-997-398; fax, +3061-993-255; e-mail, doros@sequoia.chemeng.upatras.gr).

10.1021/ma980698p CCC: $15.00
Published on Web 10/16/1998

chain systems (C_{13}, C_{44}, and C_{100}). Their results refer to conformational characteristics, and segmental and terminal relaxation. An important outcome of this work involved comparisons of simulation findings for the dynamics of chains with the predictions of the Rouse model. An analysis of the normal modes of the chains indicated that the Rouse behavior is not followed by the shorter C_{13} and C_{44} chain systems; only the longer C_{100} chain system seemed to conform to Rouse model predictions. Even for this system, however, the behavior was not exactly Rouse. Although the first three modes ($p = 1-3$) did follow the exponential decay predicted by the Rouse model, all higher modes showed clear, systematic deviations from that.[14−17] This is especially interesting in view of neutron spin−echo spectroscopy experiments, which seem to be in very good agreement with the Rouse model.[18,19]

To the best of our knowledge, C_{100} is the longest system that has been simulated so far with MD in full atomistic representation. In addition, all MD simulations seem to have been restricted to purely monodisperse melts. In the present work, new data are presented which have been collected from detailed atomistic MD simulations on polydisperse polyethylene (PE) melts. All systems studied are characterized by a uniform distribution of chain lengths with polydispersity index around 1.09. The data have been accumulated from simulations on three different systems, covering a wide range of chain lengths, up to the regime of molecular weights corresponding to formation of entanglements. The first system consists of 32 chains with mean length C_{24} (chain lengths uniformly distributed between C_{12} and C_{36}), the second of 10 chains of mean length C_{78} (chain lengths uniformly distributed between C_{39} and C_{117}), and the third of 20 chains of mean length C_{156} (chain lengths uniformly distributed between C_{78} and C_{234}).

An important aspect of the present work is that initial configurations for the MD were generated with the very efficient *end-bridging* Monte Carlo algorithm,[20] which has been shown to provide vigorous sampling of configuration space, particularly for the longer chains. At the end of an end-bridging MC simulation, the system is completely equilibrated at all length scales, from the level of the bond to the level of the chain end-to-end vector. Relaxed configurations thus obtained are subjected to MD simulation to monitor their evolution in time and extract dynamic properties. This combination of MC and MD renders MD more effective in tracking the evolution of the equilibrated system for a longer time.

The end-bridging move, invoked in the equilibrating MC runs, is a chain connectivity-altering move, which continuously generates chains of different lengths, subject to a prescribed distribution function set by a profile of relative chemical potentials. The equilibrated melts obtained from the end-bridging MC simulations are therefore polydisperse, and, of course, they continue to be so also during the MD. This is a very important feature of the present work for two reasons: (a) it allows testing the validity of the Rouse model picture that chains in the unentangled polymer regime move as strings of Brownian particles tethered by harmonic springs in a viscous medium whose interaction with the particle is characterized by a single parameter (the friction coefficient ζ); and (b) it allows studying the dynamics of many, different-length chains simultaneously, and therefore extracting the dependence of the dynamic properties on chain length without the need for different runs at different chain lengths. Of course, due to the presence of only a few chains with exactly the same length in the simulation box, the statistics for each chain length is worse than would be obtained from a monodisperse melt simulation; as we shall see, however, in the presentation of results, this does not turn out to be a significant problem.

Particular emphasis is placed in this work on the prediction of the zero-shear viscosity. As mentioned above, this technologically very important property is very difficult to predict directly for long-chain systems from equilibrium (through the Green−Kubo relation using the time integral of the shear-stress autocorrelation function) or nonequilibrium (through the response to an imposed steady shear field) dynamic simulations. The possibility of predicting the viscosity from the friction factor ζ extracted from MD simulations is explored here, and found to be very promising for sufficiently long chains.

The paper is organized as follows. Section 2 presents the molecular model used in the present work and outlines the basic characteristics of the MD algorithm. Section 3 reviews the basic assumptions and the most important equations of the Rouse model. Results from the MD simulations are presented and compared with experiments and other simulations in section 4. Finally, in section 5, the major conclusions are summarized and plans for future work are presented.

2. Molecular Model and MD Algorithm

A united-atom description of the PE melt is used in the present work, with methylene and methyl groups being modeled as single Lennard-Jones (LJ) sites.

Nonbonded interactions are described by a Lennard-Jones potential of the form

$$V_{\mathrm{LJ}}(r) = 4\epsilon\left[\left(\frac{\sigma}{r}\right)^{12} - \left(\frac{\sigma}{r}\right)^{6}\right] \tag{1}$$

with $\epsilon = 0.098$ kcal/mol and $\sigma = 3.94$ Å. These values of ϵ and σ are the same for methyl and methylene groups and equal to those used by Dodd and Theodorou.[21] $V_{\mathrm{LJ}}(r)$ describes all intermolecular site−site interactions as well as intramolecular interactions between sites separated by more than 4 bonds.

A bond-bending potential of the form[22]

$$V_{\mathrm{bending}}(\theta) = {}^1/_2 K_\theta(\theta - \theta_0)^2 \tag{2}$$

is also used for every skeletal bond angle θ, with $K_\theta = 115.2$ kcal/mol and $\theta_0 = 112°$.

Associated with each dihedral angle ϕ is also a torsional potential of the form[23]

$$V_{\mathrm{torsional}}(\phi) = c_0 + c_1\cos\phi + c_2(\cos\phi)^2 + c_3(\cos\phi)^3 + c_4(\cos\phi)^4 + c_5(\cos\phi)^5 \tag{3}$$

with $c_0 = 2.217$, $c_1 = 2.905$, $c_2 = -3.135$, $c_3 = -0.731$, $c_4 = 6.271$, and $c_5 = -7.527$ in kcal/mol.

Adjacent methyl and methylene groups along each chain backbone are maintained at a fixed distance $l = 1.54$ Å from each other. To make the model sample the configuration−space probability density characteristic of a flexible model in the limit of infinitely stiff bond stretching force constants,[24] a Fixman potential[25] is

introduced in the MD simulation. The Fixman potential for a chain of N sites numbered from 0 to $N-1$, $(N-1)$ bonds numbered from 1 to $N-1$ and $(N-2)$ bond angles numbered from 1 to $N-2$, has the form

$$V_{\text{Fixman}} = \frac{k_B T}{2} \ln[\det \mathbf{H}_N] + k_B T \ln (l_1^2 \, l_2^2 ... l_{N-1}^2) \tag{4}$$

where $l_1 = l_2 = ... = l_{N-1} = l$ are the bond lengths and $\mathbf{H}_N$ is the matrix

$$\mathbf{H}_N = \begin{pmatrix} \mu_1 & \gamma_1 & & 0 \\ \gamma_1 & \mu_2 & & 0 \\ & & 0 & 0 \\ 0 & & \mu_{N-2} & \gamma_{N-2} \\ 0 & & \gamma_{N-2} & \mu_{N-1} \end{pmatrix} \tag{5}$$

with

$$\mu_i = \frac{1}{m_{i-1}} + \frac{1}{m_i}$$
$$\gamma_i = \frac{\cos \theta_i}{m_i} \tag{6}$$

In eq 6, m_i is the mass of the ith skeletal site and θ_i the ith bond angle. The determinant $h_N = \det \mathbf{H}_N$ can be calculated recursively, through the equation

$$h_i = \mu_{i-1} h_{i-1} - (\gamma_{i-2})^2 h_{i-2} \qquad 3 \le i \le N \tag{7}$$

with $h_1 = 1$ and $h_2 = (1/m_0) + (1/m_1)$. The total Fixman potential, V_{Fixman}, is a sum of contributions of the form of eq 4 from all "parent" chains in the system. The force on any particle i in the model system due to the Fixman potential is calculated as

$$\mathbf{F}_i^{\text{Fixman}} = -\frac{\partial V_{\text{Fixman}}}{\partial \mathbf{R}_i} \tag{8}$$

with $\boldsymbol{R}_i$ the position vector of the particle, by making use of the recursive relations, eq 7. With the Fixman potential, the MD model becomes fully equivalent to that used in our end-bridging MC runs,[20] which employ the V_{LJ}, V_{bending}, and $V_{\text{torsional}}$ potentials stated above.

Results reported in this work are based on MD simulations conducted in the *NVE* equilibrium ensemble for the C_{24} and C_{78} systems, and in the *NVT* ensemble for the C_{156} system. The C_{24} and C_{78} systems were also studied in the *NVT* ensemble, and it was confirmed that the resulting dynamics was identical. In all simulations, the volume was kept constant at a value corresponding to a melt density exactly the same as the mean density obtained from the *NPT* end-bridging MC run[20] that yielded the initial configuration for the dynamic simulation. $P = 1$ atm and $T = 450$ K were used in all cases reported here.

The total duration of the MD runs was 8 ns for the C_{24} chain system, 30 ns for the C_{78} system, and about 20 ns for the C_{156} system.

In both *NVE* and *NVT* simulations, a 6th-order Gear predictor−corrector scheme was used to integrate the equations of motion in Cartesian coordinates. Constraint forces associated with the fixed bond length constraints were determined using the method of Edberg, Evans, and Morriss.[26] The code made use of a Verlet neighbor list to keep the CPU time spent in the calculation of forces at a minimum. For the larger C_{156} chain system, an additional linked-cell list was kept;[2] according to this, the simulation box is divided into $4 \times 4 \times 4$ subcells with the Verlet neighbor list searching for potential neighbors only within the 27 nearest subcells. The integration time step was always equal to 1 fs.

The simulations in the *NVT* ensemble further required the use of a Nosé−Hoover thermostat[27,28] to maintain the temperature fixed at its prescribed value. This was achieved by introducing an additional degree of freedom, s, playing the role of a heat bath, whose aim is to damp out temperature deviations from the desirable level. This necessitates adding to the total energy an additional potential term of the form

$$V_s = g k_B T \ln s \tag{9}$$

and an additional kinetic energy term of the form

$$K_s = \frac{1}{2} Q \frac{\dot{s}^2}{s} = \frac{p_s^2}{2Q} \tag{10}$$

In the above equations, g is the total number of degrees of freedom ($= 3 N_{\text{atoms}} - N_{\text{bonds}} - 3$ with N_{atoms} and N_{bonds} standing for the total numbers of atoms and bonds in the model system, respectively), while Q and p_s represent the "effective mass" and momentum, respectively, associated with the new degree of freedom s. Equations of motion are derived from the Lagrangian of the extended ensemble, including the degree of freedom s.

An important result in Hoover's analysis[28] is that the set of equations of motion is unique, in the sense that no other equations of the same form can lead to a canonical distribution. With the introduction of the Nosé−Hoover thermostat, the total Hamiltonian $H_{\text{Nosé}}$, defined as

$$H_{\text{Nosé}} = \sum_i \frac{\mathbf{p}_i^{\,2}}{2m_i} + V(\mathbf{r}) - \frac{1}{2}\sum_i \frac{\lambda_i}{2}\left((\mathbf{R_{i+1}} - \mathbf{R_i})^2 - l^2\right) + \frac{Q}{2}\left(\frac{\dot{s}}{s}\right)^2 + g\frac{\ln s}{\beta} \tag{11}$$

should be conserved during the run. The first term on the right hand side represents the kinetic energy ($\mathbf{p}_i$ is the momentum vector of site i), the second term is the potential energy (including the Fixman potential), the third term is the contribution to the Hamiltonian due to constraint bond lengths with λ_i being the Lagrange multiplier for the ith bond,[26] and the last two terms are the contributions due to the thermostat. In our MD runs, $H_{\text{Nosé}}$, was found to change by less than 1% within 1 ns of simulation.

3. The Rouse Model

The Rouse model[29,30] considers a polymer chain as a sequence of N Brownian particles (numbered 0, 1, 2, ..., $N-1$) connected by harmonic springs and moving in a viscous medium representing the background environment formed by all other chains. Hydrodynamic interactions between different springs are neglected. An important parameter in the Rouse formulation is the friction factor ζ (measured in units of mass per time), i.e., the proportionality constant between the velocity of a bead and the frictional force exerted on the bead as

it moves through the "sea" formed by all other particles in the system. Through the fluctuation−disipation theorem, ζ also defines the mean squared magnitude of the random (Langevin) force on the particle. The assumption of a harmonic potential for the interaction between adjoining particles allows the introduction of normal coordinates or modes $\mathbf{X}_p$, $p = 0, 1, 2, ..., N - 1$, each of which is capable of independent motion.

The normal coordinates can be defined in two ways; in terms of the position vectors[29] of the beads, or in terms of the connector vectors between beads;[31] the two approaches, of course, lead to consistent results. Without loss of generality, we can use the chemical methylene and methyl segments as beads to define Rouse modes in our atomistic model. The relevant formulations and the equations pertinent to each definition are shown in detail in the Appendix. If we choose to work with the position vectors, then the normal coordinates are given by

$$\mathbf{X}_p = \sum_{j=1}^{N} \Omega_{jp} \mathbf{R}_{j-1} \tag{12}$$

where Ω_{jp} are the elements of the orthogonal matrix $\mathbf{\Omega}$, given by

$$\Omega_{jp} = \sqrt{\frac{2 - \delta_{p0}}{N}} \cos\left(\frac{(j - 1/2)p\pi}{N}\right) \tag{13}$$

with $j = 1,2, ..., N$ and $p = 0, 1, ..., N - 1$, and $\mathbf{R}_i$ denotes the position vector of bead i.

With the above definition of the normal modes, the exact expression for the time autocorrelation function, $\langle \mathbf{X}_p(t) \cdot \mathbf{X}_p(0) \rangle$, of the normal mode $\mathbf{X}_p$, is given by eqs A.9 and A.10 of the Appendix. For $1 \leq p \ll N - 1$, an approximation to the exact equation can be used by taking the small $p/(N - 1)$ limit in the expression for k_p:

$$\langle \mathbf{X}_p(t) \cdot \mathbf{X}_p(0) \rangle = \frac{k_B T}{k_p} \exp\left(-\frac{t}{\tau_p}\right) = \frac{Nb^2}{6\pi^2} \frac{1}{p^2} \exp\left(-\frac{t}{\tau_p}\right) \tag{14}$$

where τ_p, $p = 1, 2, ..., N - 1$, denotes the spectrum of relaxation times,

$$\tau_p = \tau_1 / p^2 \tag{15}$$

with

$$\tau_1 = \frac{\zeta N^2 b^2}{3\pi^2 k_B T} \tag{16}$$

being the longest (or Rouse, $\tau_1 = \tau_R$) relaxation time. In the above equations, b^2 denotes the mean-square distance between adjacent beads at equilibrium. In general, $\mathbf{X}_p$ represents the local motion of a chain segment encompassing N/p beads and corresponds to motion on a length scale of the order $(Nb^2/p)^{1/2}$. The zero mode $\mathbf{X}_0$, in particular, represents the center of mass position $\mathbf{R}_G$, the mean-square displacement of which in the Rouse model is given by

$$\langle \mathbf{R}_G(t) - \mathbf{R}_G(0) \rangle^2 = 6 \frac{k_B T}{N\zeta} t \tag{17}$$

Table 1. The Mean-Square End-to-End Distance $\langle r^2 \rangle$ for Various Chain Lengths As Obtained from Bulk MD Runs, from End-Bridging MC Runs, and from MC Sampling of CUCs (P = 1 atm, T = 450 K)

$\langle r^2 \rangle$ (Å^2)	C_{46}	C_{78}	C_{84}	C_{102}	C_{117}
MD	770 ± 30	1510 ± 20	1640 ± 30	2020 ± 40	2355 ± 50
EBMC	810 ± 30	1490 ± 100	1635 ± 110	2025 ± 120	2330 ± 130
CUCs	810	1500	1624	2020	2340

From eq 17 and the Einstein relation

$$D = \lim_{t \to \infty} \frac{\langle \mathbf{R}_G(t) - \mathbf{R}_G(0) \rangle^2}{6t} \tag{18}$$

the self-diffusion coefficient of the center of mass D can be obtained as

$$D = \frac{k_B T}{N\zeta} \tag{19}$$

The Rouse model also predicts a relation for the relaxation of the time autocorrelation function of the end-to-end vector $\mathbf{r} = \mathbf{R}_{N-1} - \mathbf{R}_0$ as

$$\frac{\langle \mathbf{r}(t) \cdot \mathbf{r}(0) \rangle}{Nb^2} = \sum_{p=1,3,...} \frac{8}{p^2 \pi^2} \exp\left(-\frac{tp^2}{\tau_1}\right) \tag{20}$$

where $Nb^2 (= \langle r^2 \rangle)$ is the equilibrium (unperturbed) mean square end-to-end distance of chains in the melt. From eq 20, it is obvious that the autocorrelation function of the end-to-end vector is clearly dominated by the first ($p = 1$) mode.

The first mode defines also the zero-shear (i.e., characteristic of the Newtonian plateau) viscosity of the melt through

$$\eta_0 = \int_0^\infty G(t)\, \mathrm{d}t = \frac{\pi^2}{12} \frac{\rho R T}{M} \tau_1 \tag{21}$$

where $G(t)$ is the stress relaxation modulus, expressed as

$$G(t) = \frac{\rho R T}{M} \sum_{p=1}^{N} \exp\left(\frac{-2tp^2}{\tau_1}\right) \tag{22}$$

By combining eqs 16, 19, and 21, η_0 also becomes

$$\eta_0 = \frac{\rho R T \langle r^2 \rangle}{36 M D} \tag{23}$$

The above expressions are written in terms of the molecular weight M, the mass density of the melt ρ, and the gas constant R.

4. Results

4.1. Conformation and Local Dynamics. As a check of the correctness of the MD simulation runs, the equilibrium conformational properties of the polymer melt were first compared against those obtained from the end-bridging MC (EBMC) runs. Tables 1 and 2 present this comparison for the mean-square end-to-end distance $\langle r^2 \rangle$ of the chains and their mean-square radius of gyration $\langle s^2 \rangle$, for a variety of chain lengths. The tables also show the results obtained from MC sampling of isolated continuous unpertubed chains (CUCs).[20] The agreement between the three sets of data for both $\langle r^2 \rangle$

Table 2. The Mean-Square Radius of Gyration $\langle s^2 \rangle$ for Various Chain Lengths As Obtained from Bulk MD Runs, from End-Bridging MC Runs, and from MC Sampling of CUCs (P = 1 atm, T = 450 K)

$\langle s^2 \rangle$ (Å^2)	C_{46}	C_{78}	C_{84}	C_{102}	C_{117}
MD	107 ± 5	218 ± 10	244 ± 20	292 ± 30	335 ± 40
EBMC	112 ± 7	224 ± 10	247 ± 10	306 ± 30	360 ± 40
CUCs	111 ± 5	227 ± 10	265 ± 10	309 ± 10	333 ± 10

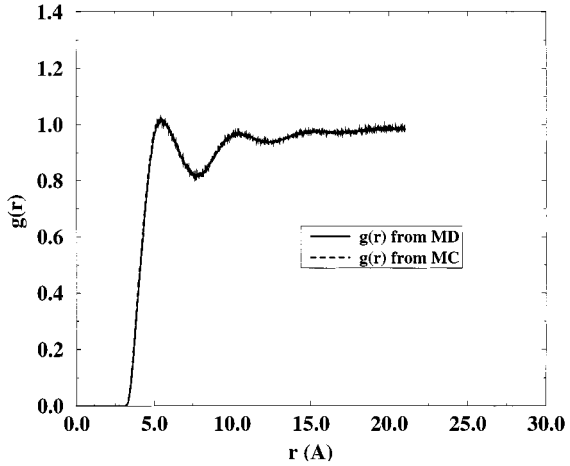

Figure 1. Intermolecular mer−mer pair distribution function, $g(r)$, for the C_{78} chain system, as obtained from the end-bridging MC (solid line) and the MD algorithm (dashed line). T = 450 K; P = 1 atm.

and $\langle s^2 \rangle$ is clear. This agreement with Flory's random coil hypothesis has been noted earlier in well-equilibrated monodisperse PE melts.[15,21] Here it is shown true for a polydisperse melt as well. One point to notice about the data of Table 1 is the large characteristic ratios to which they correspond: For the C_{102} chain, for example, C_{102} = 8.35. This value is significantly larger than the value 7.8 obtained by neutron diffraction measurements[32,33] on molten polyetehylene at 413 K. This is because the torsional potential employed in our model enhances trans conformational states.[34] Note that a recent simulation work of Yoon and collaborators,[16,17] using a different parameterization than the present work, has yielded results consistent with the measured characteristic ratios.

Figure 1 shows a comparison between the intermolecular mer−mer pair distribution functions $g(r)$ obtained from MD and EBMC. The agreement between the MC and MD simulation predictions is again excellent.

The local dynamics of the chains, particularly their torsional dynamics, can be quantified in terms of the torsion autocorrelation function, defined as

$$P(\phi(t)) = \frac{\langle \cos(\phi(t))\cos(\phi(0)) \rangle - \langle (\cos(\phi(0)))^2}{\langle \cos(\phi(0))\cos(\phi(0)) \rangle - \langle (\cos(\phi(0)))^2} \quad (24)$$

The decay of $P(\phi(t))$ is shown in Figure 2a,b. Figure 2a shows $P(\phi(t))$ for three different mean chain length systems, C_{24} (dashed line), C_{78} (solid line), and C_{156} (long-dashed line). The figure shows quite evidently that the local dynamics is faster in the small-molecular weight system, C_{24}, and slower in the large-molecular weight system, C_{156}. The decay of $P(\phi(t))$ for the C_{78} system is also shown in Figure 2b (solid line); also shown in the same figure (dashed line) is its best fit with a stretched exponential function of the form:

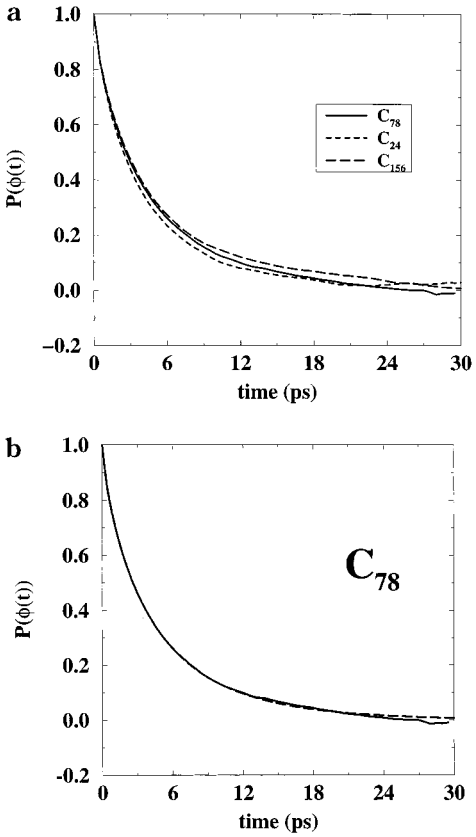

Figure 2. Torsional time autocorrelation function (a) for three mean chain length systems, C_{78} (solid line), C_{24} (dashed line) and C_{156} (long-dashed line) and (b) for the C_{78} chain system (solid line) and its stretched exponential fit (dashed line). T = 450 K; P = 1 atm.

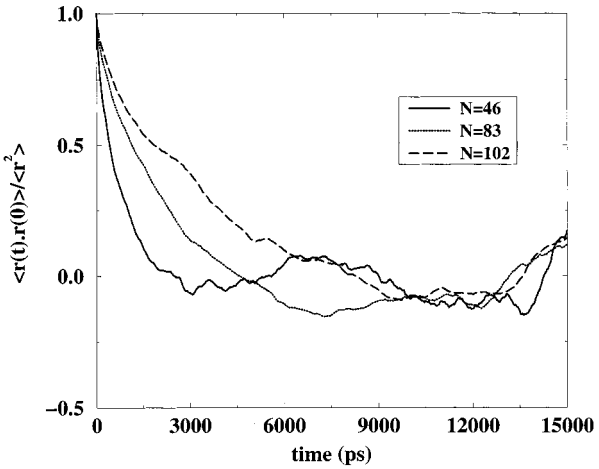

Figure 3. Time autocorrelation function for the chain end-to-end vector for various chain lengths N at T = 450 K and P = 1 atm.

$P(\phi(t)) = \exp(-(t/t_c)^{\beta})$. The characteristic relaxation time obtained by the fitting is t_c = 4.2 ps and the stretching exponent β = 0.8. The correlation time (integral under curve) is 4.6 ps.

4.2. Terminal Relaxation Properties. Figure 3 presents the decay of the orientational autocorrelation function for the end-to-end vector $\langle \mathbf{r}(t)\cdot\mathbf{r}(0) \rangle / \langle \mathbf{r}^2 \rangle$ as a function of time for three chain lengths (C_{46}, C_{83}, and C_{102}). These chain lengths were tracked in the system with mean molecular weight C_{78}. The rate at which $\langle \mathbf{r}(t)\cdot\mathbf{r}(0) \rangle / \langle \mathbf{r}^2 \rangle$ approaches the zero value is a measure of how fast the chain "forgets" its initial configuration,

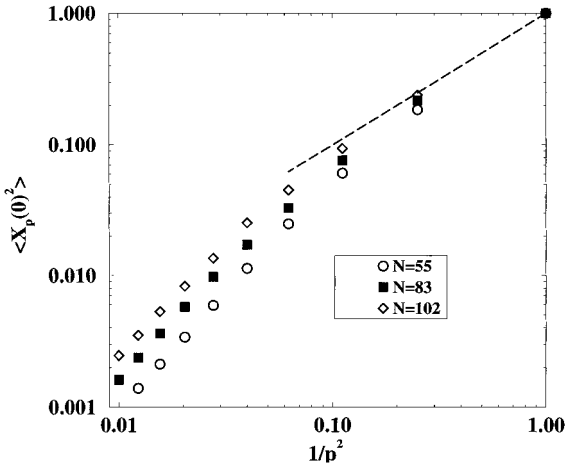

Figure 4. Normal-mode analysis. The squared amplitudes of the Rouse normal modes $\langle X_p(0)^2\rangle$ are shown as a function of the inverse squared mode number p in log−log coordinates for C_{55}, C_{83}, and C_{102} chains. The dashed line is drawn with a slope of −1, corresponding to the Rouse model.

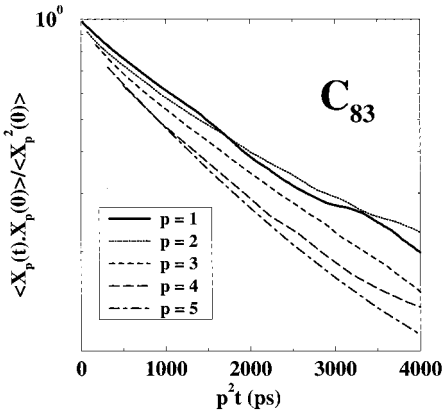

Figure 5. Normal-mode analysis. Time autocorrelation functions of the first five normal modes versus p^2t. Chain length $N = 83$; $T = 450$ K; $P = 1$ atm.

i.e., of the rate of overall relaxation of the chain. As we can see in the figure, in order for the quantity $\langle \mathbf{r}(t)\cdot\mathbf{r}(0)\rangle/\langle \mathbf{r^2}\rangle$ to reach zero (which corresponds to full relaxation of the chains) approximately 1.5 ns are needed for the C_{46} chains. For the C_{83} chains this time increases to about 4.5 ns, and for the C_{102} chains to 9 ns. This fast rise of the relaxation time with chain length shows very convincingly how difficult it is for MD to relax the conformational characteristics of chains with more than about 100 carbon atoms along their backbone.

The results of the normal mode analysis based on the Rouse model are shown in Figures 4−7. Figure 4 shows the mean squared amplitudes $\langle X_p(0)^2\rangle$ as a function of $1/p^2$, for three different chain lengths, C_{55}, C_{83}, and C_{102}. According to the Rouse model, eq 14, $\langle X_p(0)^2\rangle$ should be proportional to $1/p^2$. From the figure it is obvious that this scaling is followed only for the first two normal modes, almost exactly for $N = 102$, and only approximately for $N = 83$ and $N = 55$; the third as well as all higher modes do not follow the Rouse scaling. The deviation from Rouse scaling decreases with increasing chain length. In fact, higher modes for short chains seem to follow a much stronger dependence on p, approximately of the form $1/p^3$, as has also been reported in a recent paper by Paul et al.[17]

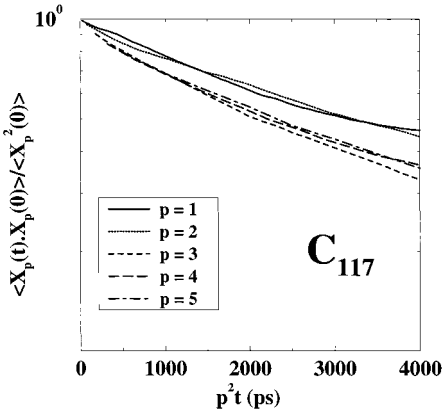

Figure 6. Normal-mode analysis. Time autocorrelation function of the first five normal modes versus p^2t. Chain length $N = 117$; $T = 450$ K; $P = 1$ atm.

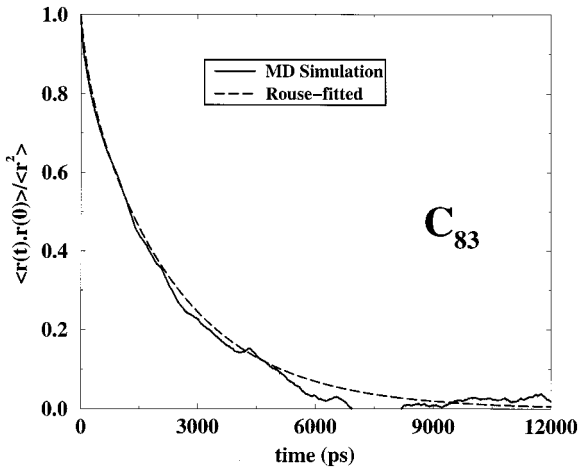

Figure 7. Time autocorrelation function for the chain end-to-end vector as extracted directly from the simulation (solid line) and as calculated from the Rouse model using the τ_1 value derived from the normal-mode analysis. Chain length $N = 83$; $T = 450$ K; $P = 1$ atm.

Figures 5 and 6 show the logarithm of the normalized time autocorrelation function $\langle \mathbf{X_p}(t)\cdot\mathbf{X_p}(0)\rangle/\langle \mathbf{X_p}(0)^2\rangle$ as a function of p^2t for the modes $p = 1-5$, and for two different chain lengths, C_{83} and C_{117}. If the chains behaved identically as Rouse chains at all length scales, then, according to eqs 14 and 15, all lines on each graph should have collapsed onto a single straight line. This is not seen in Figures 5 and 6: Only the first two modes ($p = 1$ and 2) fall on the same line, which is straight to a good approximation; all higher modes, including the $p = 3$ mode, show clear deviations from Rouse scaling. The deviations are, in fact, more pronounced for the shorter C_{83} chains than for the C_{117} chains. The origin of these deviations should be sought in the length scale of the motion to which higher modes correspond: As p increases, the subchain whose relaxation is described by the pth mode gets smaller and smaller and the Gaussian assumption provides only a poor representation of the conformational statistics of such subchains. This also justifies the smaller deviations seen in the case of C_{117} chains.

By fitting the simulation results for each mode between $p = 1$ and $p = 5$ to an exponential function, estimates of the relaxation times τ_p were obtained. Of greatest importance, of course, is the value of the longest time τ_1, since this (a) governs the long length scale relaxation of the chain, and (b) defines, through eq 21,

Table 3. The Three First Relaxation Times τ_p and Their Ratios for Various Chain Lengths As Obtained from Bulk MD Runs (P = 1 atm, T = 450 K)

	C_{46}	C_{83}	C_{91}	C_{102}	C_{117}
τ_1 (ps)	800 ± 100	2800 ± 100	3600 ± 200	4200 ± 200	4800 ± 400
τ_2 (ps)	230 ± 30	860 ± 70	890 ± 60	920 ± 70	1040 ± 100
τ_3 (ps)	90 ± 10	285 ± 20	350 ± 20	380 ± 30	450 ± 80
τ_1/τ_2	3.5 ± 0.63	3.3 ± 0.29	4.05 ± 0.35	4.5 ± 0.41	4.6 ± 0.65
τ_1/τ_3	8.9 ± 1.49	9.8 ± 0.9	10.3 ± 0.82	11.0 ± 1.02	10.7 ± 2.2

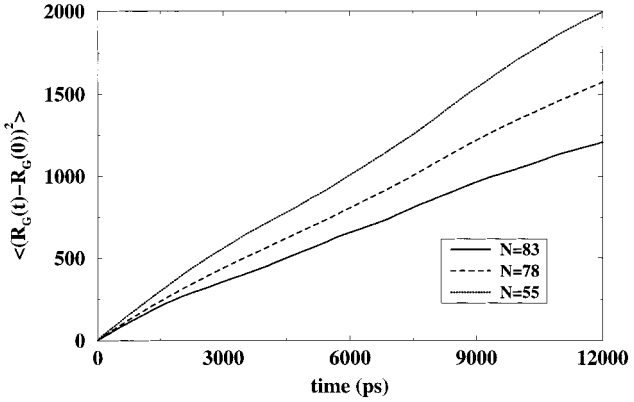

Figure 8. The chain center-of-mass mean-square displacement as a function of time for three chain lengths: C_{83} (solid line), C_{78} (dashed line), and C_{55} (dotted line).

the viscosity of the melt. According to eq 16, τ_1 should increase quadratically with chain length N. The data reported in Table 3 show an increase of τ_1 with chain length N which is almost quadratic, mainly for the longer chains. According to eq 15, τ_p should be proportional to the inverse squared order of the normal mode p. This means that the ratios τ_1/τ_2 and τ_1/τ_3 should assume values of 4 and 9, respectively. From Table 3 one can see that the ratio τ_1/τ_2 is roughly 4 for almost the entire range of chain lengths present in our system, within the error bars of the simulation. This ratio clearly exhibits an increasing tendency with increasing chain length, suggesting a slight departure of the second mode from the Rouse prediction. The ratio τ_1/τ_3, on the other hand, is significantly larger than 9 for most chain lengths, suggesting that chains are too short for their third mode to behave in a Rouse-like fashion.

One way to check the validity of the picture of exponentially decaying modes is to reconstruct the time autocorrelation function for the chain end-to-end vector, eq 20, and compare it with that obtained directly from the MD simulation. The case of C_{83} chains is shown in Figure 7: The solid line represents the curve obtained from the simulation while the dashed line shows the reconstructed curve based on the first 5 normal modes, using the τ_1 values reported in Table 3 and eq 15. The figure shows that the Rouse model reproduces quite faithfully the simulation curve, and this indicates that the model can reliably capture the long- (if not the short-) time dynamics of chains.

The self-diffusion behavior of the chains is examined in Figure 8, which shows a typical plot of the mean-square displacement of the chain center of mass $\langle(R_G(t) - R_G(0))^2\rangle$ for three different chain lengths (C_{55}, C_{78}, and C_{83}) as a function of time t. In the small-time regime (times shorter than the longest relaxation time), a non-Fickian, subdiffusive behavior is observed, where $\langle(R_G(t) - R_G(0))^2\rangle \propto t^{0.8}$, as has already been observed in other simulations, both with atomistic[17] and with coarse-grained models.[3] In the long-time ($t > \tau_1$) regime, however, a linear dependence of $\langle(R_G(t) - R_G(0))^2\rangle$ on t is indeed seen, and this permits the calculation of the self-diffusion coefficient D through the Einstein relation. By repeating the procedure for various chain lengths, D can be tabulated as a function of N; the results are shown in Table 4.

Values of the segmental friction coefficient ζ_D extracted from D through eq 19 are shown in the fifth row of Table 4. Estimates of the same quantity ζ_τ, extracted from the Rouse times listed in the first row of Table 4 through eq 16, are shown in the fourth row of the same table. Estimates of the zero-shear rate viscosity obtained from ζ_D using eq 23 of the Rouse model are listed in the sixth row of Table 4. In the third and seventh row of Table 4 experimental data[35] for D and η_0 are shown for almost monodisperse low-molecular weight polyethylene melts found in the literature.

The first point to notice about the data presented in Table 4 is the very good agreement between simulation and experimental values for the self-diffusion coefficient D: Both for the C_{46} and C_{90} chains considered, the experimentally measured values are very close to the simulation results. An interesting point to remark concerns the friction coefficient ζ: Although the two values, ζ_τ and ζ_D, obtained from τ_1 and D, respectively, show some deviations for the shorter chains, for the longer chains they fall within the error bars of each other. This can be seen better in Figure 9, where ζ is plotted as a function of N: The friction coefficient ζ_D and ζ_τ values are low and different from each other in the short-chain regime ($N < 40$), but exhibit common values for longer chains. We regard the values of ζ_D as more representative of the melts studied; they can be obtained with less statistical error from the simulation trajectories, rely merely on the Einstein equation for the diffusivity (eq 19), and are therefore less dependent on the validity of the Rouse model. As N increases and the Rouse model gets more and more representative of the actual system, the two values ζ_D and ζ_τ should come closer; the figures do support this. On the other hand, according to the Rouse model, ζ should be a constant, independent of chain length. The results of our MD simulations show that this is not true: According to Figure 9, ζ_D becomes independent of chain length N only for chains longer than C_{70}. More specifically, Figure 9 shows that ζ increases from a small value (close to 0.15 $\times 10^{-9}$ dyn s/cm) representative of a short-chain alkane-like behavior, to a plateau value (around 0.45 $\times 10^{-9}$ dyn s/cm) characteristic of the long-chain Rouse behavior. This is an important result of the present work, since it defines the threshold in chain length, above which the Rouse model should be expected to provide a realistic description of the dynamics of an unentangled polymer melt. One should note that the points displayed in Figure 9 were obtained from systems of various sizes and mean chain lengths. The points with $N \leq 46$ were obtained from the system with mean length C_{24}, the points with $46 \leq N \leq 117$ were obtained from the system with mean length C_{78}, and finally the last two points were obtained from the system with mean

Table 4. Friction Coefficient ζ, Self-Diffusivity D, and Zero-Shear Rate Viscosity η_0 versus Chain Length

	C_{46}	C_{83}	C_{90}	C_{117}	C_{128}	C_{144}
τ_1 (ps)	800 ± 100	2800 ± 200	3600 ± 300	4800 ± 500	7500 ± 400	10000 ± 500
D (10^{-6} cm^2/s)	4.0 ± 0.2	1.98 ± 0.1	1.46 ± 0.1	1.16 ± 0.2	1.0 ± 0.1	0.93 ± 0.1
D_{exp} (10^{-6} cm^2/s)	4.6		1.4			
ζ_τ (10^{-9} dyn s/cm)	0.39 ± 0.04	0.386 ± 0.04	0.42 ± 0.04	0.32 ± 0.06	0.425 ± 0.04	0.44 ± 0.04
ζ_D (10^{-9} dyn s/cm)	0.34 ± 0.05	0.38 ± 0.04	0.47 ± 0.05	0.46 ± 0.06	0.48 ± 0.04	0.47 ± 0.04
η_0 (cp)	1.46 ± 0.07	5.8 ± 0.03	8.6 ± 0.5	12.9 ± 1.5		
$\eta_{0,exp}$ (cp)	2.5		9.2			

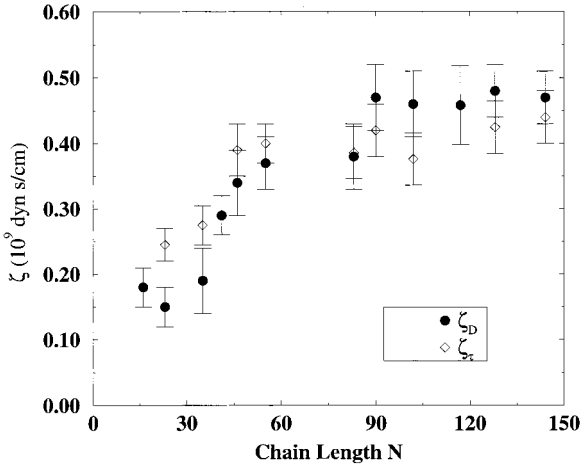

Figure 9. The friction coefficient ζ versus chain length N, as obtained from the Rouse relation between ζ and diffusion coefficient D (ζ_D, full symbols) and from the Rouse relation between ζ and the longest relaxation time τ_1 (ζ_τ, open symbols).

chain length C_{156}. For some points (for example C_{90} and C_{102}), ζ were extracted from both the C_{78} and C_{156} mean chain length systems; these values were found practically identical. This proves that the friction factors are not significally affected by mean molecular weight and system size at these chain lengths. Additional evidence for the system size independence of our results comes from the following observation: Running the C_{78} simulation with the same molecular weight distribution in a box four times larger than the one for which results are reported here[34] yielded identical dynamics for all chain lengths.

Of great importance is the calculation of the zero-shear viscosity η_0 from the simulations and its comparison with experimental data. In contrast to D, which is a primary property obtained directly from the simulation, η_0 is evaluated by invoking the Rouse model, eq 21. Therefore, η_0 should be expected to be predicted reliably only for those chain lengths for which the Rouse model also provides a valid description of the system, i.e., for $N > 60-70$. This explains the large difference observed between the calculated and the experimentally measured η_0 values for the C_{46} chains, but it also justifies the very good agreement seen for the longer C_{90} system. Unfortunately, no experimental values of η_0 were found in the literature for chains longer than C_{90} and shorter than C_{150} with which to compare our simulation results.

5. Conclusions

Results have been presented for the dynamic properties of linear PE melts of uniform chain length distribution and polydispersity index 1.09 for a variety of mean chain lengths from detailed atomistic MD simulations. Before subjecting the systems to the MD simulation, exhaustive equilibration at all length scales was achieved by use of the end-bridging MC algorithm. A wide range of chain lengths, ranging from C_{20} to about C_{150}, have been analyzed for times longer than about 12 ns to calculate reliably their dynamic properties.

The most significant result of this work is the evaluation of the friction coefficient ζ, an important mesoscopic parameter invoked by the Rouse model to describe the interactions of the chain backbone with the viscous medium. The dependence of ζ on chain length has been extracted by mapping MD trajectories onto the Rouse model. The simulation results demonstrated the presence of a minimum chain length value around C_{60}, above which ζ can be considered as a constant, chain length independent parameter of the system. In the regime of chain lengths corresponding to this constant, asymptotic value of ζ, the zero-shear viscosity η_0 was calculated from the Rouse model and found to be in excellent agreement with measured values. Results were also presented for the self-diffusivity D as a function of chain length; these were found to be within a few percent of the experimentally measured values.

In the future, results from MD simulations of strained preoriented configurations will be presented and compared with the present data. Results will also be presented for chain lengths greater than C_{150}, corresponding to the onset of the entangled regime.

Acknowledgment. This work was supported by the European Commission through BRITE/EuRam Project BRPR-CT96-0145. We are also indebted to the San Diego Supercomputer Center for a generous allocation of time on the Cray T90. We gratefully acknowledge the General Secretariat of Research and Technology of Greece for partial support in the form of a PENED '95 Program, No. 218.

Appendix. Normal Modes

The normal coordinates in the Rouse model can be defined using either the position vectors $\mathbf{R}_i$ ($i = 0, 1, ..., N - 1$) or the connector vectors $\mathbf{Q}_i \equiv \mathbf{R}_i - \mathbf{R}_{i-1}$ ($i = 1, ..., N - 1$) of the beads. Although both definitions should lead to consistent results, as they involve a linear transformation between the two sets of vectors, the final equations for the time autocorrelation functions of the normal modes present some differences, which will be reported in this Appendix.

The first way to define the normal coordinates is through the position vectors,[29,36] through eqs 12 and 13 of the main text. The eigenvalues of $\mathbf{\Omega}$ are given by

$$\lambda_p = 4 \sin^2\left(\frac{p\pi}{2N}\right) \qquad p = 0, ..., N - 1 \qquad \text{(A.1)}$$

The second way is to define the normal coordinates through the connector vectors:[31]

$$\mathbf{X}_p = \sum_{i=1}^{N-1} \Omega'_{jp} \mathbf{Q}_j \qquad \text{(A.2)}$$

where Ω'_{jp} are the elements of the orthogonal matrix $\mathbf{\Omega}'$, given by

$$\Omega'_{jp} = \sqrt{\frac{2}{N}} \sin\left(\frac{jp\pi}{N}\right) \qquad \text{(A.3)}$$

with $j = 1, ..., N - 1$ and $p = 1, ..., N - 1$. The eigenvalues of $\mathbf{\Omega}'$ are given by

$$\lambda'_p = 4 \sin^2\left(\frac{p\pi}{2N}\right) \qquad p = 1, ..., N - 1 \qquad \text{(A.4)}$$

Note that $\mathbf{\Omega}'$ is a $(N - 1) \times (N - 1)$ matrix, whereas $\mathbf{\Omega}$ is a $N \times N$ matrix. On the other hand, the matrix $\mathbf{\Omega}$ is singular, its first eigenvalue being zero and all its nonzero eigenvalues coinciding with those of $\mathbf{\Omega}'$.

The analysis to find the time autocorrelation function of the normal modes proceeds by transforming the Langevin equation for the position vectors to a corresponding equation for the normal coordinates, using the orthogonality property of the matrices $\mathbf{\Omega}$ or $\mathbf{\Omega}'$. An important step in the transformation procedure is the way in which the random forces on the beads are transformed from the original to the eigenvector space. If, for example, $\mathbf{f}_n$ is the random force on bead n in the original Cartesian space, then the existence of a friction factor ζ for the interaction of beads with the viscous medium implies that[30]

$$\langle f_{n\alpha}(t)\, f_{m\beta}(t')\rangle = 2\zeta k_B T \delta_{nm} \delta_{\alpha\beta} \delta(t - t') \qquad \text{(A.5)}$$

To be able to derive the time autocorrelation function for the normal modes, a similar expression should be written for the transformed force $\mathbf{f}_p$ on mode p, that is, we assert that there exists a friction constant ζ_p such that

$$\langle f_{p\alpha}(t)\, f_{q\beta}(t')\rangle \equiv 2\zeta_p k_B T \delta_{pq}\, \delta_{\alpha\beta} \delta(t - t') \qquad \text{(A.6)}$$

The task therefore is to find the relation between ζ_p and ζ for the two definitions of the normal modes. In the case where the normal modes are defined on the basis of the position vectors of the beads, it is found that[30]

$$\zeta_p = \frac{2N\zeta}{(1 + \delta_{p0})} \qquad \text{(A.7)}$$

In the case where the normal modes are defined on the basis of the connector vectors of the beads, following an approach similar to the one outlined in ref 30, it is found that

$$\zeta_p = \frac{N\zeta}{(1 + \delta_{p0})\left(1 - \cos\left(\frac{p\pi}{N}\right)\right)} \qquad \text{(A.8)}$$

After having defined the relation between ζ_p and ζ, the time autocorrelation function for the normal modes is written as

$$\langle X_{p\alpha}(t)\, X_{q\beta}(0)\rangle = \delta_{pq}\, \delta_{\alpha\beta} \frac{k_B T}{k_p} \exp\left(-\frac{t}{\tau_p}\right) \qquad \text{(A.9)}$$

where k_p ($p = 1, 2, ..., N - 1$) is found from the spring constant $k = (3k_B T)/b^2$ of the Rouse chain as

$$k_p \equiv k \frac{\zeta_p}{\zeta} \sin^2\left(\frac{p\pi}{N}\right) \qquad \text{(A.10)}$$

Since two different expressions are found for ζ_p, depending on the definition of the normal modes, k_p is also different.

Since k_p defines the magnitude of the normal modes and not their time evolution, the two alternative definitions differ only in the dependence of the intensity of the normal modes on the mode number: According to the first definition, $\langle X_p(0)^2\rangle \propto 1/p^2$ for $p \ll N$, but according to the second definition it is the quantity $(1 - \cos(p\pi/N))\ \langle X_p(0)^2\rangle$ which is proportional to $1/p^2$. Although the normal mode analysis results reported in the main body of this paper have all been based on the first definition, exploratory calculations with the second definition were found to conform perfectly to the scalings reported in this Appendix.

With regard to the definition of the spectrum of relaxation times and the exponential decay of the normal modes, the two definitions produce identical results, because these depend on the ratio ζ_p/k_p, which is the same in the two cases. The corresponding equations were given in section 3 of the paper.

References and Notes

(1) Allen, M. P.; Tildesley, D. J. *Computer Simulation of Liquids*; Oxford University Press: Oxford, 1987.
(2) Frenkel, D.; Smit, B. *Understanding Molecular Simulations: From Algorithms to Applications*; Academic Press: New York, 1996.
(3) Binder, K., Ed. *Monte Carlo and Molecular Dynamics Simulations in Polymer Science*; Oxford University Press: New York, 1995.
(4) Witner, U.; Paul, W.; Binder, K. *Macromolecules* **1992**, *25*, 7211.
(5) Kremer, K.; Grest, G. *J. Chem. Phys.* **1990**, *92*, 5057.
(6) Weber, T. A. *J. Chem. Phys.* **1978**, *69*, 2347; **1979**, *70*, 4271.
(7) Jin, Y.; Pernice, M.; Boyd, R. *Comput. Theor. Polym. Sci.* **1996**, *6*, 9.
(8) Brown, J.; Clarke, G. *J. Chem. Phys.* **1994**, *100*, 1684; **1996**, *104*, 2078.
(9) Xu, Z.; de Pablo, J.; Kim, S. In press.
(10) Xu, Z.; de Pablo, J.; Kim, S. *J. Chem. Phys.* **1995**, *102*, 5836.
(11) Daivis, P. J.; Evans, D. J. *J. Chem. Phys.* **1995**, *103*, 4261.
(12) Cui, S. T.; Gupta, S. A.; Cummings, P. T.; Cohran, H. D. *J. Chem. Phys.* **1996**, *105*, 1214.
(13) Mondello, M.; Grest, G. *J. Chem. Phys.* **1995**, *103*, 7156; **1997**, *106*, 9327.
(14) Smith, G.; Yoon, D. Y. *J. Chem. Phys.* **1994**, *100*, 649.
(15) Smith, G.; Yoon, D. Y. *J. Chem. Phys.* **1995**, *103*, 1702.
(16) Han, J.; Jaffe, R. L.; Yoon, D. Y. *Macromolecules* **1997**, *30*, 7245.
(17) Paul, W.; Smith, G. D.; Yoon, D. Y. *Macromolecules* **1997**, *30*, 7772.
(18) Richter, D.; Ewen, B.; Farago, B.; Wagner, T. *Phys. Rev. Lett.* **1989**, *62*, 2140.
(19) Richter, D.; Willner, L.; Zirkel, A.; Farago, B.; Fetters, L. J.; Huang, J. S. *Macromolecules* **1994**, *27*, 7437.
(20) Pant, P. V. K.; Theodorou, D. N. *Macromolecules* **1995**, *28*, 7224.
(21) Dodd, L. R.; Theodorou, D. N. *Adv. Polym. Sci.* **1994**, *116*, 249.
(22) Van der Ploeg, P.; Berendsen, H. J. C. *J. Chem. Phys.* **1982**, *76*, 3271.
(23) Ryckaert, J. P.; Bellemans, A. *Chem. Phys. Lett.* **1975**, *30*, 123.
(24) Gō, N.; Scheraga, H. A. *Macromolecules* **1976**, *9*, 535.
(25) Fixman, M. *Proc. Nat. Acad. Sci.* **1974**, *71*, 3050.
(26) Edberg, R.; Evans, D. J.; Morriss, G. P. *J. Chem. Phys.* **1986**, *84*, 6933.
(27) Nosé, S. *Mol. Phys.* **1984**, *52*, 255.
(28) Hoover, W. G. *Phys. Rev. A* **1985**, *31*, 1695.

(29) Rouse, P. E. *J. Chem. Phys.* **1953**, *21*, 1272.
(30) Doi, M.; Edwards, S. F. *The Theory of Polymer Dynamics*; Claredon: Oxford, 1986.
(31) Bird, B. R.; Curtiss, C. F.; Armstrong, R. C.; Hassager, O. Kinetic Theory, *Dynamics of Polymer Liquids*, 2nd ed.; Wiley: New York, 1987.
(32) Horton, J. C.; Squires, G. L.; Boothroyd, A. T.; Fetters, L. J.; Rennie, R. J.; Glinka, C. J.; Robinson, R. A. *Macromolecules* **1989**, *22*, 681.
(33) Fetters, L. J.; Graessley, W. W.; Krishnamoorti, R.; Lohse, D. J. *Macromolecules* **1997**, *30*, 4973.
(34) Mavrantzas, V. G.; Theodorou, D. N. *Macromolecules* **1998**, *31*, 6310.
(35) Pearson, D. S.; Ver Strate, G.; Von Meerwall, E.; Schilling, F. C. *Macromolecules* **1987**, *20*, 1133.
(36) Verdier, P. H. *J. Chem. Phys.* **1966**, *45*, 2118.

MA980698P